REFERENCES AND NOTES

1. M. B. Sporn and D. L. Newton, *Fed. Proc.* **38**, 2528 (1979).
2. T. Kudo, T. Narisawa, S. Abo, *Gann* **71**, 260 (1980); M. Pollard, P. H. Luckert, M. A. Schmidt, *Cancer Lett.* **21**, 57 (1983); W. R. Waddell, G. R. Ganser, E. J. Cerise, R. W. Loughry, *Am. J. Surg.* **157**, 175 (1989); M. J. Thun, M. M. Namboodiri, C. W. Heath, *N. Engl. J. Med.* **325**, 1593 (1991).
3. O. J. Plescia, A. H. Smith, K. Grinwich, *Proc. Natl. Acad. Sci. U.S.A.* **72**, 1848 (1975); J. S. Goodwin, *Am. J. Med.* **77**, 7 (1984).
4. T. V. Zenser *et al.*, *J. Pharmacol. Exp. Ther.* **227**, 545 (1983); D. Wild and G. H. Degan, *Carcinogenesis* **8**, 541 (1987).
5. Roots of *C. quinquangulata* Rich. (Leguminosae) were collected in Peru in 1974. The dried ground plant material (1 kg) was extracted twice overnight with methanol at room temperature, followed by concentration and dilution with water to give a water-methanol solution (1:9, v/v). After washing with hexane, this methanolic layer was partitioned with ethyl acetate. The ethyl acetate extract (90 g) (88% inhibition of COX activity at 69 μg/ml) was separated into 28 fractions with chloroform-methanol (0 to 30% methanol) as eluent over a silica gel chromatographic column. Fractions 13 to 17 (66 to 85% inhibition of COX activity at 69 μg/ml) were combined (4 g), and this material was subjected to further column chromatography. The column was developed with chloroform-methanol (1 to 15% methanol) and hexane-ethyl acetate (3:1 to 1:1) to afford an active compound (30 mg, 0.003%) that was determined to be $C_{14}H_{12}O_3$ by high-resolution mass spectral (MS) analysis. This compound was identified as resveratrol by comparison of its physical data and ^{1}H–nuclear magnetic resonance (NMR), ^{13}C-NMR, and MS data with those of an authentic sample [E. Mannila, A. Talvitie, E. Kolehmainen, *Phytochemistry* **33**, 813 (1993); G. S. Jayatilake *et al.*, *J. Nat. Prod.* **56**, 1805 (1993)]. Additional resveratrol for the studies here was purchased from Sigma (St. Louis, MO). The commercial material was evaluated by high-pressure liquid chromatography coupled with MS analysis and found to be pure.
6. L. W. Wattenberg, *Cancer Res.* **53**, 5890 (1993).
7. J. K. Gierse *et al.*, *Biochem. J.* **305**, 479 (1995).
8. S. Sharma, J. D. Stutzman, G. J. Kelloff, V. E. Steele, *Cancer Res.* **54**, 5848 (1994). HL-60 cells were maintained in RPMI 1640 medium (Gibco BRL, Grand Island, NY) supplemented with 5% heat-inactivated calf serum, penicillin G sodium (100 U/ml), and streptomycin sulphate (100 μg/ml) (Gibco BRL) at 37°C in a humidified atmosphere at 5% CO_2 in air. Differentiation was induced by a 7-day treatment with 1.3% dimethyl sulfoxide (DMSO), and the cells were cultured in 96-well plates (1×10^6 cells per well) in Hanks' balanced salt solution containing 30 mM Hepes, pH 7.6. After the addition of TPA (8 μM) to induce free radical formation, cytochrome c (160 μM) and resveratrol were added. The cells were incubated for 1 hour at 37°C, and antioxidant activity was determined by monitoring absorbance at 550 nm. The same reaction mixture, without the HL-60 cells, was used as a blank control.
9. L. A. Shamon *et al.*, *Anticancer Res.* **14**, 1775 (1995). A reaction mixture was prepared containing *Salmonella typhimurium* strain TM677, S9 liver homogenate derived from Aroclor 1254-pretreated rats, a NADPH-generating system (NADPH is the reduced form of nicotinamide adenine dinucleotide phosphate), and various concentrations of resveratrol, which were added 1 min before the addition of 80 μM DMBA. After incubation for 2 hours at 37°C, the bacteria were recovered by centrifugation, resuspended, and plated (in triplicate) on minimal agar in the presence or absence of 8-azaguanine. The plates were then incubated for 48 hours at 37°C, and the results were expressed as mutant fractions, that is, the average number of colonies capable of growing in the presence of 8-azaguanine divided by the average number of colonies capable of growing in the absence of 8-azaguanine, after correcting for dilution factors. The percent inhibition was calculated relative to control plates that were treated with DMSO only.
10. H. J. Prochaska and A. B. Santamaria, *Anal. Biochem.* **169**, 328 (1988).
11. Y. Zhang, T. W. Kensler, C.-G. Cho, G. H. Posner, P. Talalay, *Proc. Natl. Acad. Sci. U.S.A.* **91**, 3147 (1994).
12. N. Suh, L. Luyengi, H. H. S. Fong, A. D. Kinghorn, J. M. Pezzuto, *Anticancer Res.* **15**, 233 (1995).
13. R. C. Moon and R. G. Mehta, in *Chemistry and Biology of Retinoids*, M. I. Dawson and W. H. Okamura, Eds. (CRC Press, Boca Raton, FL, 1990), pp. 501–518.
14. W. Dercks and L. L. Creasy, *Physiol. Mol. Plant Pathol.* **34**, 289 (1989).
15. P. Jeandet, R. Bessis, B. Gautheron, *Am. J. Enol. Vitic.* **42**, 41 (1991); E. H. Siemann and L. L. Creasy, *ibid.* **43**, 49 (1992); D. M. Goldberg *et al.*, *ibid.* **46**, 159 (1995).
16. A. I. Romero-Pérez, R. M. Lamuela-Raventós, A. L. Waterhouse, M. C. de la Torre-Boronat, *J. Agric. Food Chem.* **44**, 2124 (1996).
17. E. B. Rimm *et al.*, *Lancet* **338**, 464 (1991); A. L. Klatsky, M. A. Armstrong, G. D. Friedman, *Ann. Intern. Med.* **117**, 646 (1992); A. L. Klatsky, *Clin. Exp. Res.* **18**, 88 (1994).
18. D. M. Goldberg, S. E. Hahn, J. G. Parkes, *Clin. Chim. Acta* **237**, 155 (1995).
19. H. Arichi *et al.*, *Chem. Pharm. Bull.* **30**, 1766 (1982); Y. Kimura, H. Lkuda, S. Arichi, *Biochim. Biophys. Acta* **834**, 275 (1985); C. R. Pace-Asciak *et al.*, *Clin. Chim. Acta* **235**, 207 (1995).
20. Daily consumption of two to five glasses (or a maximum of 375 ml/day) of red wine may deliver a sufficient amount of resveratrol to alter arachidonic acid metabolism or other physiological responses, depending on absorption, metabolism, and residence time within the blood circulation and relevant tissues [D. M. Goldberg, *Clin. Chem.* **41**, 14 (1995)]. Resveratrol concentrations in other food products, such as grape juice, pomace, and purees are provided in B. J. Ector, J. B. Magee, C. P. Hegwood, and M. J. Coign [*Am. J. Enol. Vitic.* **47**, 57 (1996)].
21. F. J. G. Van der Ouderaa and M. Muytenhek, *Methods Enzymol.* **86**, 60 (1982); R. J. Kulmacz and E. M. Lands, in *Prostaglandins and Related Substances. A Practical Approach*, C. Benedetto, R. G. McDonald-Gibson, S. Nigam, T. F. Slater, Eds. (IRL Press, Oxford, 1987), pp. 209–227.
22. K. Slowing, E. Carretero, A. Villar, *J. Ethnopharmacol.* **43**, 9 (1994). Female Wistar rats (150 to 200 g body weight) were divided into groups of seven animals each. All rats received 0.1 ml of Freund's complete adjuvant (Difco; Sigma) by intradermal injection into the tail. Animals were used 7 days after injection of adjuvant. One hour after oral administration of resveratrol (3 or 8 mg per kilogram of body weight) or reference drugs including phenylbutazone (80 mg/kg) and indomethacin (5 mg/kg), the rats were injected with 0.1 ml of a 2% (w/v) suspension of carrageenan in saline solution into the left hind paw. For the control group, a 1:1 mixture of Tween 80 and water (0.2/3.3, v/v) and 1% (w/v) methylcellulose was used as a vehicle. The left hind paw volume of each rat was measured by water plethysmography (Letica, model L17500) before the adjuvant injection and, again, 6 days later, before the injection of carrageenan. Paw volumes were determined within 3 to 144 hours after injection of carrageenan. Inhibition of edema was calculated relative to the mean edema of the vehicle-treated control group.
23. C. Gerhäuser *et al.*, *Nature Med.* **1**, 260 (1995).

24. We thank N. Suh, S. K. Lee, C. Gerhäuser, L. A. Shamon, M. Hawthorne, and D. D. Lantvit for technical assistance; W. G. Thilly for *S. typhimurium* strain TM677; J. P. Whitlock for Hepa 1c1c7 and BP^{r}C1 cells; H. Constant for HPLC-MS analysis of resveratrol; and J. K. Gierse for COX-2. Supported by grant P01 CA48112 from the National Cancer Institute.

9 July 1996; accepted 8 October 1996

Synaptic Depression and Cortical Gain Control

L. F. Abbott,* J. A. Varela, Kamal Sen, S. B. Nelson

Cortical neurons receive synaptic inputs from thousands of afferents that fire action potentials at rates ranging from less than 1 hertz to more than 200 hertz. Both the number of afferents and their large dynamic range can mask changes in the spatial and temporal pattern of synaptic activity, limiting the ability of a cortical neuron to respond to its inputs. Modeling work based on experimental measurements indicates that short-term depression of intracortical synapses provides a dynamic gain-control mechanism that allows equal percentage rate changes on rapidly and slowly firing afferents to produce equal postsynaptic responses. Unlike inhibitory and adaptive mechanisms that reduce responsiveness to all inputs, synaptic depression is input-specific, leading to a dramatic increase in the sensitivity of a neuron to subtle changes in the firing patterns of its afferents.

Cortical neurons transmit information by responding selectively to changes in the spatial and temporal pattern of presynaptic action potentials arriving at about 10,000 synapses. Extracting meaningful information from such a large and complex set of inputs presents a severe challenge. Presynaptic afferents fire action potentials at a wide variety of different rates, and signals carried by slowly firing afferents may be masked by random fluctuations in the activity of afferents firing at high rates. This problem can be avoided if cortical neurons monitor slowly firing afferents at high gain while reducing the gain for high-rate inputs. Such gain control cannot be achieved through fixed synaptic weights, because afferent firing rates change over time. We propose that short-term synaptic depression provides an automatic, dynamic gain-control mechanism. By balancing contributions

L. F. Abbott and Kamal Sen, Volen Center, Brandeis University, Waltham, MA 02254, USA.
J. A. Varela and S. B. Nelson, Department of Biology, Brandeis University, Waltham, MA 02254, USA.
*To whom correspondence should be addressed.

from slowly and rapidly firing afferents, synaptic depression increases the sensitivity of cortical neurons to small rate changes and other fluctuations in afferent firing patterns that could not otherwise be detected.

Intracortical synapses display several forms of facilitation and depression (*1*–*3*). We have measured and characterized synaptic transmission along a major excitatory pathway (layer 4 to layer 2/3) in slices of rat primary visual cortex (*3*, *4*). Upon repeated stimulation, the predominant form of short-term plasticity displayed by these synapses is depression that develops over the first few action potentials and recovers in less than a second. Figure 1A shows the onset of depression and Fig. 1B the steady-state amplitude as a function of rate for field potentials evoked by repetitive stimulation. Both extracellular and intracellular recordings of responses to fixed-rate and random Poisson spike trains were used to construct a model of depression at these synapses (*5*) that accurately fits the experimental results for both random and fixed-rate spike trains. In the model, short-term depression is described by decrementing the amplitude of the postsynaptic response by a multiplicative factor f, falling in the range of $0.65 < f < 0.86$, whenever the presynaptic neuron fires an action potential. Between action potentials, the amplitude recovers exponentially back toward its initial value with time constant τ, with 200 ms $< \tau <$ 600 ms (*6*). For constant input firing rate r, the normalized steady-state amplitude $A(r)$ (Fig. 1B) decreased as a function of r and was approximately proportional to $1/r$ for large rates (*7*).

With depressing synapses, the total steady-state synaptic conductance resulting from a set of afferents firing at rate r is proportional to $rA(r)$ (if we make the approximation that synapses add linearly), the product of the rate and the steady-state amplitude (Fig. 1B, dashed curve). At high rates where $A(r) \sim 1/r$, this approaches a constant value and the total steady-state synaptic conductance arising from multiple depressing synapses loses its dependence on rate (*8*). This loss of sensitivity to sustained rates is accompanied by an increase in the sensitivity to abrupt changes in rate. If a steady presynaptic firing rate r changes suddenly by an amount Δr, the first action potentials at the new rate will be transmitted with amplitude $A(r)$ before depression further modifies synaptic strength. Thus, the magnitude of the transient synaptic conductance will be proportional to $\Delta r A(r)$. Because $A(r)$ decreases as a function of rate, afferents that are firing rapidly are deemphasized relative to those firing slowly. Specifically, because $A(r)$ is roughly proportional to $1/r$, the transient synaptic conductance evoked by a rate change Δr is approximately proportional to $\Delta r/r$. This is reminiscent of the Weber-Fechner law in psychophysics stating that the perceived magnitude of a change ΔI in the intensity I of a stimulus is proportional to $\Delta I/I$ (*9*). Synaptic depression realizes a similar Weber-Fechner relation at the level of individual synapses. This produces a transient synaptic response roughly proportional to the percentage change of the input firing rate.

Experimental data verified that the amplitudes of transient synaptic responses evoked by constant percentage changes of input firing rates are insensitive to rate for rates above about 10 Hz (Fig. 1C). In this range, the transient response amplitude was indeed proportional to the fractional change $\Delta r/r$ of the stimulation rate; the amplitude for $\Delta r/r = 1$ was twice as big as that for $\Delta r/r = 0.5$ (Fig. 1C). By contrast, fixed-amplitude rate changes produced responses that decreased as a function of rate (Fig. 1D). Without synaptic depression, the response would be constant for fixed-amplitude rate changes and would grow linearly with rate for fixed percentage changes.

To study the gain control provided by synaptic depression, we constructed a model integrate-and-fire neuron (*10*) with half its synapses receiving action potentials at a high rate (100 Hz) and half at a low rate (10 Hz). The responses of the model neuron to a 2-Hz modulation of the firing rates of each set of afferents (Fig. 2A) show the equalizing effects of synaptic depression. Without depressing synapses, 50% modulation of the rapidly firing afferents affected the firing output of the model neuron, but 50% modulation of the slowly firing afferents did not (Fig. 2B). With synaptic depression, 50% modulation of either the rapidly or slowly firing inputs had a strong impact on the response of the neuron (Fig. 2C). As well as amplifying the effect of large percentage changes on slowly firing afferents, synaptic depression allows small percentage fluctuations of rapidly firing inputs to be ignored. This is important because random fluctuations of high average firing rates involve large absolute variations (*11*). The same $\pm$5-Hz modulation that strongly affected the neuronal response when it occurred on slowly firing afferents (Fig. 2C, middle panel) had no observable effect when applied to the rapidly firing inputs (Fig. 2C, right panel).

Despite the reduction of synaptic strength at sustained high presynaptic rates, neurons with depressing synapses can still exhibit selective steady-state responses. Although depressing synapses collectively convey little information about the magnitude of high presynaptic firing rates, information about which afferents are firing rapidly is not lost, and this is sufficient for selectivity. We computed the steady-state firing rate of a neuron that is selectively tuned to the value of a variable x representing some encoded attribute of a sensory

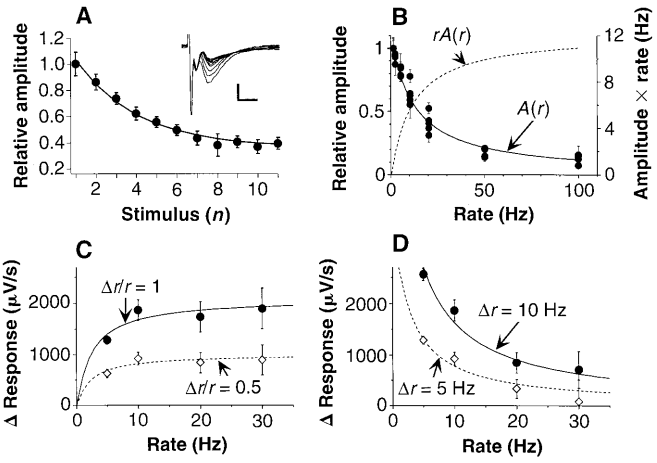

Fig. 1. Experimental results and fits of the model for synaptic depression. (**A**) Depression of synaptic responses during repetitive stimulation. Filled circles indicate normalized average field potential amplitudes evoked by 11 consecutive stimuli at 20 Hz. Error bars are standard deviations over five repetitions. The solid curve is the fit of the model. Mean responses are shown in the inset (scale: 200 μV, 5 ms). The three downward deflections in each trace were identified in separate experiments (*3, 4*) as a stimulus artifact, an antidromic response, and an excitatory synaptic response. The amplitude of the antidromic response does not change systematically over the course of the stimulations, indicating that the effectiveness of axonal stimulation was constant. (**B**) The normalized steady-state amplitude of field potentials after 15 stimuli at rates from 1 to 100 Hz. The plotted points are from five separate experiments, and error bars indicate standard deviations over five trials. The solid curve is the fit of the model. The dashed curve (right-hand axis) shows the product of the steady-state amplitude times the stimulation rate. (**C** and **D**) After repetitive stimulation at rate r, the stimulation rate was increased to $r + \Delta r$. The plotted points show the change in the product of the amplitude of the field potential times the rate of stimulation. (C) Results and fit of the model for constant percentage rate changes ($\Delta r/r$ = constant). Filled circles show the results for $\Delta r/r = 1$ and open diamonds for $\Delta r/r = 0.5$. Solid and dashed curves are the corresponding model fits. (D) Same as in (C), but for fixed amplitude rate changes (Δr = constant). Filled circles show the results for $\Delta r = 10$ Hz and open diamonds for $\Delta r = 5$ Hz.

stimulus. The model neuron receives input from a large array of afferents firing at rates that are Gaussian functions of x peaked at different values of x for different afferents (Fig. 3A, inset). The synaptic weights connecting these afferents to the postsynaptic neuron are adjusted to make its firing rate a Gaussian function of x peaked at zero (*12*).

Synaptic depression broadened the tuning of the steady-state response by reducing the sensitivity to sustained afferent firing rates, but it did not eliminate selectivity (Fig. 3A). Furthermore, synaptic depression greatly increased the sensitivity of the model neuron to sudden small changes, Δx, in the value of x (Fig. 3B, solid line). In the absence of depression, this sensitivity, defined as the change in firing rate divided by Δx, is equal to the slope of the response tuning curve (Fig. 3B, dashed line). However, with depression, the sensitivity was more than twice the magnitude of the slope of the steady-state tuning curve. Synaptic depression increases sensitivity by decreasing the gain for rapidly firing afferents that are insensitive to small Δx, giving slower firing afferents with more sensitivity a larger impact. The sensitivity of both the afferents and the postsynaptic neuron in this example is largest at the point where the slope of the tuning curve is maximal. Thus, the afferents are most sensitive to small changes in x not when they are firing fastest, but when they fire at moderate rates where their Gaussian tuning curves are steepest.

The enhanced sensitivity resulting from synaptic depression extends to more complex input fluctuations as well. There is experimental evidence that the firing rates of cortical neurons are statistically fairly independent (*13*). Thus, it is interesting to examine neuronal responses to an uncorrelated combination of rate increases on some afferents and rate decreases on others. We did this by studying an integrate-and-fire neuron receiving Poisson afferent spike trains at a variety of rates. Each afferent rate was chosen independently from a probability distribution (*14*). We examined the sensitivity of the model neuron to uncorrelated changes in afferent firing rates by suddenly choosing a new set of afferent rates from the same underlying probability distribution. The rate changes we consider are thus synchronous in time but uncorrelated in amplitude.

Neurons without depressing synapses respond primarily to the average firing rate of all their afferents. Input fluctuations involving a large number of uncorrelated afferent rate changes have a relatively small effect on the average firing rate. The relative magnitude of the transient synaptic conductance induced by synchronous uncorrelated firing rate changes on n afferents decreases like $1/\sqrt{n}$ with nondepressing synapses (Fig. 3C) (*15*). Like responses to asynchronous uncorrelated afferent fluctuations (that is, noise), the resulting responses are small if n is large (*11*). Consequently, a neuron with nondepressing synapses cannot detect synchronous uncorrelated presynaptic rate changes (Fig. 3D).

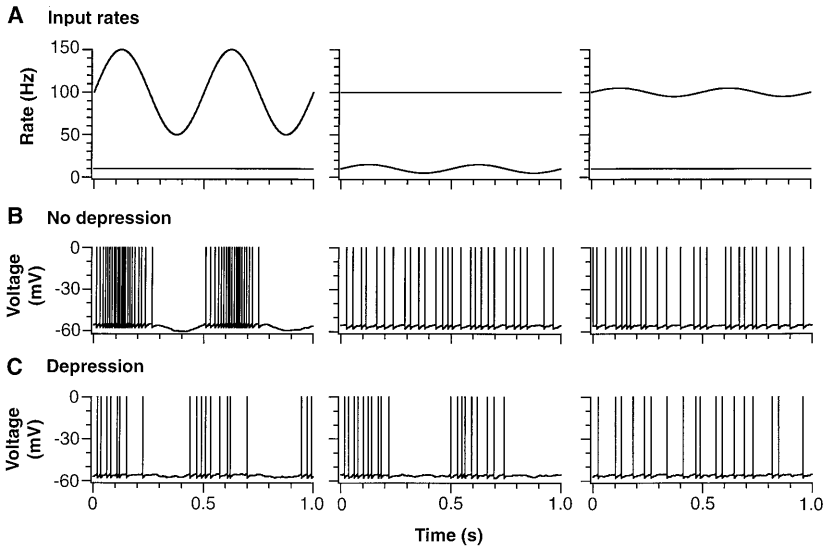

Fig. 2. Response of an integrate-and-fire model neuron receiving 100 synaptic inputs each with mean rate of 100 Hz and 100 inputs each with mean rate of 10 Hz. (**A**) Input rates for the two sets of synapses used to generate the responses in (B) and (C). (Left) the firing rates of the rapidly firing inputs are modulated by 50% while the 10-Hz inputs are held at constant rate. (Center) One hundred–hertz inputs are constant; slowly firing afferents are modulated by 50%. (Right) Ten-hertz inputs are constant and 100-Hz inputs are modulated by ±5 Hz. (**B**) The responses of an integrate-and-fire model neuron without synaptic depression to the input modulation shown in (A) above each panel. Only 50% modulation of the 100-Hz inputs affects the firing pattern (left). The firing in the center and right panels is indistinguishable from that produced by unmodulated 10- and 100-Hz inputs. (**C**) Response of the same model neuron but with synaptic depression to the input modulations shown in (A). A 50% modulation of 100-Hz (left) and 10-Hz (center) inputs affects the firing pattern similarly, whereas ±5-Hz amplitude modulation applied to rapidly firing inputs has no observable effect (right).

The situation is completely different with depressing synapses. Here, a synchronous uncorrelated change of input firing rates produced a change in synaptic conductance that was independent of the number of afferents (Fig. 3C). With synaptic depression, a change of input rates evokes a large transient response even if the average presynaptic firing rate remains constant. This occurs when synapses that were formerly firing at low rates and are relatively undepressed, suddenly fire at high rates. As a result, synchronous uncorrelated rate changes induce transient responses (Fig. 3E) much larger than those produced by asynchronous noise. Synchronous uncorrelated rate changes may thus be a significant source of the observed variability in neural responses, and they could represent an important element of the neural population code. Afferents can carry the maximum amount of information if their rates are statistically independent or nonredundant, forming a factorial code (*16*). Synaptic depression gives a neuron access to such a code by allowing it to respond to uncorrelated afferent rate changes.

In many situations, the optimal configuration for extracting information from a set of afferents may involve synapses exhibiting different amounts of short-term depression (*17*), and such a range is seen in the data (*1–3, 8*). Manipulations that increase or decrease transmitter release modify the onset rate of synaptic depression, but have little effect on steady-state synaptic strengths (*18*). Examples include changes in extracellular Ca^{2+} (*3, 8*), a form of long-term potentiation (*2*), and presynaptic neuromodulation by adenosine and acetylcholine (*3, 8*). Thus, the temporal characteristics of synaptic depression can be tuned while retaining the basic gain-control mechanism we have been discussing.

Many cortical neurons respond vigorously to transient inputs but weakly, or not at all, to sustained excitation (*19*). Synaptic depression may contribute to the transient nature of cortical responses. Like other forms of short-term plasticity, synaptic depression causes the response of a cortical neuron to depend on the previous history of afferent firing. As a result, neuronal responses reflect the current state of presynaptic activity within the context of previous activity. This enhances neuronal sensitivity to both correlated and uncorrelated syn-

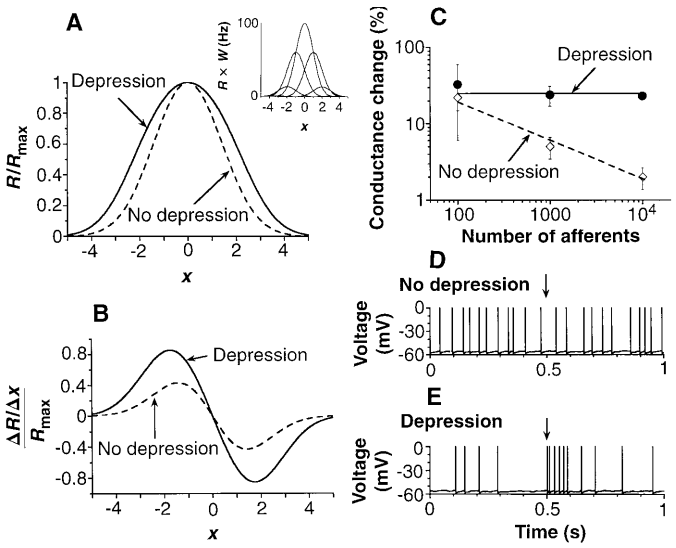

Fig. 3. (**A**) The firing-rate response curve for a model neuron receiving inputs from afferents tuned to the value of a sensory attribute x. The inset shows a few representative afferent firing rate tuning curves multiplied by the synaptic weight factors used for them in the model. The dashed curve is the resulting firing rate of the postsynaptic neuron in the absence of synaptic depression. Synaptic depression (solid curve) broadens the response but does not eliminate tuning. The plotted curves show the firing rate divided by its maximum value R_{max}. (**B**) The sensitivity of the model neuron to sudden changes of x by an amount Δx. This is defined as the rate change ΔR evoked by a given Δx divided by $\Delta x R_{max}$. This sensitivity is independent of Δx for small Δx, but it depends on the initial value of x either without depression (dashed curve) or with depression (solid curve). (**C** through **E**) The neuronal response of a model integrate-and-fire neuron (*10*) to synchronous uncorrelated input rate changes. The magnitude of transient synaptic conductance changes arising from synchronous uncorrelated rate changes on different number of afferents is shown (C). Each second, input rates were randomly rechosen from an exponential probability distribution. Filled circles show the root-mean-square amplitude of the resulting transient conductance change averaged over 100 ms after the rate changes. Error bars indicate the standard deviation over 10 trials. Open diamonds and dashed line give the result without synaptic depression, and the change in conductance falls as one over the square root of the number of afferents. Filled circles and solid line show the result with depression and the conductance change is independent of the number of afferents. Without depression (D), a sudden uncorrelated change of 1000 afferent rates at the time indicated by the arrow has no impact on the firing of the model neuron. With depression (E), the model neuron produces a strong transient response to a synchronous uncorrelated rate change involving 1000 afferents (arrow).

chronous input fluctuations and greatly expands the range of possible coding strategies for cortical neurons.

REFERENCES AND NOTES

1. R. Deisz and D. Prince, *J. Physiol.* (*London*) **412**, 513 (1989); S. B. Nelson and D. Smetters, *Soc. Neurosci. Abstr.* **19**, 629 (1993); A. M. Thomson and J. Deuchars, *Trends Neurosci.* **17**, 119 (1994); K. J. Stratford, K. Tarczy-Hornoch, K. A. C. Martin, N. J. Bannister, J. J. B. Jack, *Nature* **382**, 258 (1996).
2. H. Markram and M. Tsodyks, *Nature* **382**, 807 (1996).
3. S. B. Nelson, J. A. Varela, J. Gibson, K. Sen, L. F. Abbott, *Soc. Neurosci. Abstr.* **22**, 952 (1996); S. B. Nelson, J. A. Varela, K. Sen, L. F. Abbott, in *Proceedings of Computational Neuroscience-96*, J. Bower, Ed., July 96, in press. These experiments revealed several components of short-term plasticity: rapid facilitation recovering in 50 to 150 ms, rapid depression with a 200- to 600-ms recovery time, and slower depression lasting 5 to 10 s. At high frequencies (above about 50 Hz) an additional very rapid depression is also evident. For the phenomena we consider here, the dominant form of short-term plasticity is well described by a single component of effective depression.
4. Slices of rat primary visual cortex (400 μm thickness) were prepared from Long Evans rats (age 17 days to adult) by use of standard methods. Experiments were performed at 35°C. Transillumination was used to visualize the boundaries of primary visual cortex and the border between layers 2/3 and 4. Field potentials (n = 50 slices) were recorded with saline-filled pipettes, amplified by 10,000, filtered at 1 to 1000 Hz, and digitized with Pulse Control software [J. Herrington, K. R. Norton, R. J. Bookman (Univ. of Miami Press, Miami, FL, 1994)]. Trains of electrical stimuli (10 to 150 μA, biphasic, 80 μs) were applied via a monopolar stimulating electrode placed in layer 4 immediately below the recording site in layer 2/3. Stimulus artifacts and antidromic and synaptic responses were differentiated on the basis of latency and effects of tetrodotoxin, which blocks antidromic and synaptic responses, and 6-cyano-7-nitroquinoxaline-2,3-dione (CNQX), which blocks synaptic but not antidromic responses. Synaptic amplitudes were measured from the peak of the initial response, because slopes were often contaminated by antidromic responses. In several experiments in which antidromic responses were clearly separated from initial slopes, we confirmed that analysis of initial slopes and peaks yielded nearly identical measures of short-term plasticity [see V. Aroniadou and T. Teyler, *Brain Res.* **562**, 136 (1991); G. Hess, C. D. Aizenman, J. P. Donoghue, *J. Neurophysiol.* **75**, 1765 (1996)]. Changes in synaptic responses were not due to reduced polysynaptic contributions, because 50 to 90% reduction in response amplitude with 0.2 to 0.5 mM CNQX, which greatly decreases polysynaptic activation, produced no change in synaptic depression (n = 5). Synaptic responses recorded intracellularly in layer 2/3 in response to layer 4 stimulation (n = 14 cells) matched the latencies, time courses, and short-term plasticity observed in field-potential recordings (*3*).
5. This model is related to the analysis of K. L. Magleby and J. E. Zengel, *J. Gen. Physiol.* **80**, 613 (1982). We have modeled all the forms of short-term plasticity seen at these synapses (*3*), but use a simpler one-component model here.
6. The specific parameter values used for the examples in this paper are f = 0.75 and τ = 300 ms, obtained from the fit of Fig. 1B. The results we present do not depend critically on the precise values of these parameters; any values within the observed ranges produce qualitatively similar results.
7. $A(r)$ is computed by noting that, at steady state, the amplitude takes the same value at every spike. Immediately before a spike, the synaptic amplitude is A. This is multiplied by f, and by the time of the next spike, recovers exponentially to $1 + (fA - 1)\exp(-1/r\tau)$. Setting these two expressions equal to each other gives $A(r) = [1 - \exp(-1/r\tau)]/[1 - f\exp(-1/r\tau)]$. For large rates and $f \neq 1$, we use the approximation $\exp(-1/r\tau) \approx 1 - 1/r\tau$ to obtain $A(r) \approx 1/(1 - f)r\tau$.
8. Tsodyks and Markram have independently reached this conclusion and have considered its functional implications. [M. V. Tsodyks and H. Markram, in *Lecture Notes in Computer Science*, C. von der Malsburg, W. von Seelen, J. C. Vorbrüggen, B. Sendhoff, Eds. (Springer, Berlin, 1996), pp. 445–450; *Proc. Natl. Acad. Sci. U.S.A.*, in press].
9. G. J. Fechner, *Elemente der Psychophysik* (Breitkopf and Härtel, Leipzig, Germany, 1880); S. S. Stevens, in *Handbook of Perception*, E. C. Carterett and M. P. Friedman, Eds. (Academic Press, New York, 1974), vol. 2, pp. 361–389. This relation holds for a variety of sensory modalities and presumably arises from multiple neuronal mechanisms at both peripheral and central levels. The similar behavior of synaptic and perceptual responses need not imply a causal relationship. Rather, these may represent similar solutions to the problem of processing inputs with wide dynamic ranges. If responses proportional to $\Delta I/I$ are established at the periphery, transient responses of central neurons driven through depressing synapses will be proportional to $\Delta I/I$ divided by the firing rate of their afferents. Because the peripheral firing rate depends only logarithmically on I, the presence of depressing central synapses will have minimal impact on a Weber-Fechner relation established at the periphery.
10. All simulations use a single compartment integrate-and-fire neuron with a resting potential of −70 mV and a membrane time constant of 30 ms. Synapses are represented as conductance changes with a reversal potential of 0 mV. Upon arrival of a presynaptic spike, the conductance rises instantaneously to a value $g\alpha$, where g is a constant (the same for all synapses) and α describes the depression at the synapses receiving the spike. The synaptic conductance decays back to zero with a time constant of 2 ms. Presynaptic spike trains were generated from a Poisson distribution. The factor α obeys the differential equation $\tau d\alpha/dt = 1 - \alpha$ and is multiplied by f whenever a presynaptic spike occurs. When the membrane potential reaches −55 mV, the model neuron fires a spike and is reset to −58 mV. For Fig. 2, the model neuron had 200 synapses with g = 0.075 when depression was included and g = 0.0125 without depression. For Fig. 3, C through E, we used g = 0.027 with depression and g = 0.013 without depression. These adjustments were made to keep the firing rates in roughly the same range for all cases. All synaptic conductances are given in units of the resting membrane conductance.
11. W. R. Softky and C. Koch, *Neural Comp.* **4**, 643 (1992); *J. Neurosci.* **13**, 334 (1994).
12. In the model, the firing rate of 500 afferents determines the firing rate of a single postsynaptic neuron. The firing rate of afferent i responding to the value x is given by $r_i = (100\text{ Hz})\exp[-(x - x_i)^2/2]$. The values of the afferent tuning curve peaks, x_i, are spread uniformly in the range from −10 to 10. The firing rate of the postsynaptic neuron is given by $R = \Sigma_i W_i A(r_i) r_i$ where $A(r)$ is the steady-state amplitude in (*7*). The synaptic weight factor is $W_i = \exp(-x_i^2/2)$.
13. T. J. Gawne and B. J. Richmond, *J. Neurosci.* **13**, 2758 (1993); T. J. Gawne, T. W. Kjaer, J. A. Hertz, B. J. Richmond, *Cereb. Cortex* **6**, 482 (1996).
14. We used an exponential distribution with a mean of 10 Hz for all inputs, but similar results can be obtained with any reasonable distribution.
15. To keep the average synaptic conductance constant as the number of synapses, n, was varied, the synaptic weight factor g was set proportional to $1/n$. Other scalings of g are possible [see for example M. N. Shadlen and W. T. Newsome, *Curr. Opin. Neurobiol.* **4**, 569 (1994); M. Tsodyks and T. J. Sejnowski, *Network* **6**, 1 (1995); T. W. Troyer and K. D. Miller, *Neural Comp.*, in press] but these do not alter the amplitude of the responses to synchronous uncorrelated rate changes relative to those evoked by

asynchronous uncorrelated changes (noise).
16. H. B. Barlow, *Neural Comp.* **1**, 295 (1989); ———, T. P. Kaushal, G. J. Mitchison, *ibid.*, p. 412.
17. L. F. Abbott, K. Sen, J. A. Varela, J. Gibson, S. B. Nelson, *Soc. Neurosci. Abstr.* **22**, 952 (1996).
18. Such manipulations change the value of the parameter f in the model. The steady-state amplitude is proportional to $1/(1 - f)r$ for large r (*7*). The factor f can be considered to be the fraction of releasable transmitter remaining after a spike, so $1 - f$ is the fraction of transmitter released. The steady-state synaptic strength is gA with g proportional to the amount of transmitter released, and thus to $1 - f$. As a result, the effective synaptic strength for sustained high rates is proportional to $(1 - f)/(1 - f)r = 1/r$ and is independent of f.
19. See for example R. C. deCharms and M. M. Merzenich, *Nature* **381**, 610 (1996).
20. Care and use of animals were in accordance with the guidelines of the Brandeis University animal care committee. We thank P. Dayan, E. Marder, K. Miller, and G. Turrigiano for helpful comments and advice. Supported by the Sloan Center for Theoretical Neurobiology at Brandeis University; NSF grants IBN-9421388, DMS-9503261, and IBN-9511094; a Sloan Research Fellowship; and the W. M. Keck Foundation.

6 August 1996; accepted 14 November 1996

Circadian Rhythms in Rapidly Dividing Cyanobacteria

Takao Kondo,* Tetsuya Mori, Nadya V. Lebedeva, Setsuyuki Aoki, Masahiro Ishiura, Susan S. Golden

The long-standing supposition that the biological clock cannot function in cells that divide more rapidly than the circadian cycle was investigated. During exponential growth in which the generation time was 10 hours, the profile of bioluminescence from a reporter strain of the cyanobacterium *Synechococcus* (species PCC 7942) matched a model based on the assumption that cells proliferate exponentially and the bioluminescence of each cell oscillates in a cosine fashion. Some messenger RNAs showed a circadian rhythm in abundance during continuous exponential growth with a doubling time of 5 to 6 hours. Thus, the cyanobacterial circadian clock functions in cells that divide three or more times during one circadian cycle.

Circadian rhythms, oscillations of biological activities with a periodicity of approximately 24 hours in a constant environment, are observed in almost all organisms (*1*). The cellular components responsible for these rhythms and for the cell division cycle represent two major cellular oscillations that coexist in biological systems. The circadian clock is not a product of the cell division cycle because nondividing tissues such as the nervous tissue or mature leaves display robust circadian rhythms (*1*). However, it is unknown whether a circadian oscillation can exist when the cell division period is shorter than the circadian period. The circadian clock is thought to be dependent on state variables—that is, substances that reflect time, whose concentrations might be disrupted by the cell division process. Because several clock models implicate intracellular membrane structure directly or indirectly as a factor in circadian timing (*2*), it is important to investigate the relation between the cell cycle and circadian period. Autonomous models dependent on a clock gene, its mRNA, and its protein product have been proposed for the circadian clocks of *Drosophila* and *Neurospora* (*3*). These models assume that an important timing mechanism of a circadian feedback loop is the transport of a clock protein from the cytoplasm, where it is synthesized, to the nucleus, where it affects expression of its own gene. Cell division, which disrupts and divides the nuclear structure, might interfere with such a mechanism.

Stable circadian rhythms have been observed only in cells that divide more slowly than the circadian period. In *Tetrahymena* and *Euglena*, a circadian rhythm of cell division observed in slow-growing cultures does not persist when the generation time is less than a day (*4*). We used a transformed reporter strain (AMC149) of the cyanobacterium *Synechococcus* sp. PCC 7942 (*5*, *6*) to study circadian rhythms because it can divide much more rapidly than the circadian frequency and its circadian rhythm of bioluminescence can be monitored with high precision. A bacterial luciferase reporter gene inserted into the chromosome in AMC149 expresses a circadian bioluminescence rhythm. AMC149 displays a circadian rhythm that is physiologically equivalent to those of many eukaryotes (*7*). The generation time of *Synechococcus* can be as rapid as 5 to 6 hours and can be controlled easily by changing the light fluence or temperature. Here we demonstrate that cultures of cyanobacteria that divide twice or more per day display circadian rhythms of bioluminescence and levels of mRNA.

During an early stage of liquid culture, *Synechococcus* grew exponentially until the density reached 5×10^7 cells per milliliter (*8*). Because the optical density at 730 nm (OD_{730}) of the culture was below 0.05, the effective light intensity was not lowered by self-shading (*9*). Microscopic observation confirmed that *Synechococcus* also grew ex-

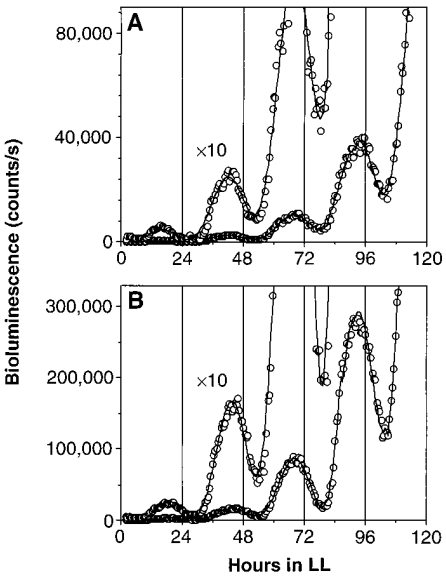

Fig. 1. Bioluminescence rhythm (open circles) and theoretical curve (solid lines) for exponentially growing *Synechococcus* in liquid culture and on an agar plate. (**A**) Measurements in liquid medium. AMC149 cells were cultured in modified BG11 medium (*13*) under LL to a density of 10^9 cells per milliliter. The culture was then diluted to 10^5 cells per milliliter. (**B**) Measurements on solid medium. Cells were spread on a 1-cm^2 area of an agar plate to form 1000 to 3000 microcolonies. (A and B) After 12 hours of darkness, a 1-ml aliquot of liquid culture or 1-cm^2 area of agar was transferred to a 20-ml vial, and 0.2 ml of 0.5% *n*-decanal solution (dissolved in oil) was placed in the vial separately. The bioluminescence from the vials was monitored continuously by the automated system with a photon-counting photomultiplier (*10*). The light fluence rate was 46 μE m^{-2} s^{-1} during LL, and temperature was continuously maintained at 30°C. Bioluminescence from the vials is plotted against time in LL by open circles without a connecting line. The bioluminescence data were analyzed by Igor software (*11*) to find a best-fit curve to a model equation. Theoretical curves are superimposed in each plot. To visualize the profile of low-level bioluminescence during the early phase of each experiment, a 10-fold expansion of the bioluminescence is shown in each panel (×10 curve).

T. Kondo, S. Aoki, M. Ishiura, Division of Biological Science, Graduate School of Science, Nagoya University, Chikusa, Nagoya, 464-01 Japan.
T. Mori, Department of Biology, Vanderbilt University, Nashville, TN, 37235, USA.
N. V. Lebedeva and S. S. Golden, Department of Biology, Texas A&M University, College Station, TX, 77843, USA.
*To whom correspondence should be addressed.